

Initiating and monitoring the evolution of single electrons within atom-defined structures

Mohammad Rashidi^{1,2,3*}, Wyatt Vine^{1*}, Thomas Dienel^{1,2*}, Lucian Livadaru³, Jacob Retallick⁴, Taleana Huff^{1,3}, Konrad Walus⁴, Robert A. Wolkow^{1,2,3}

¹Department of Physics, University of Alberta, Edmonton, AB, Canada, T6G 2R3

²Nanotechnology Initiative, Edmonton, AB, Canada, T6G 2M9

³Quantum Silicon, Edmonton, AB, Canada, T6G 2M9

⁴Department of Electrical and Computer Engineering, University of British Columbia, Vancouver, BC, Canada, V6T 1Z4

*Authors contributed equally

Correspondence to: rashidi@ualberta.net, wyattvine@gmail.com, thdienel@gmail.com

Atomic manipulation^{1,2} has emerged as a powerful strategy to fabricate novel atomic physical-systems³⁻⁵ and devices⁶⁻⁸. An important addition to this experimental toolkit would be the ability to design and control functional atomic charge configurations with single electron precision. To this end, several studies have demonstrated the ability to create, move, and controllably switch charged species on a surface with scanning probe techniques⁹⁻¹⁵. While elegant, these studies have relied on large perturbative fields applied by the probe naturally impeding their use in the investigation of systems where charge states are loosely bound and prevents the generalization of results to systems in the absence of a probe. Here, we use atomic manipulation to design symmetric and asymmetric confining potentials and demonstrate methods to controllably position and track single electrons within these structures. With these techniques we prepare specific charge states of atomically engineered structures and non-perturbatively observe their field-free temporal evolution. Combining our approach with existing atomic manipulation techniques presents new opportunities for simulating designer Hamiltonians.

We investigate atom defined charge configurations composed of patterned silicon dangling bonds on a hydrogen-terminated Si(100)-2x1 surface¹⁶. The charge states of dangling bonds are isolated from the host silicon because their energy levels reside within the band gap¹⁷, eliminating the need for an insulating film between structure and substrate, which was essential in previous studies^{9-11,14,18,19}. The crystalline lattice of the substrate and the ability to selectively re-hydrogenate dangling bonds ensures the perfect spacing of substituent atoms and the ability to create error free designer structures²⁰⁻²². Recent non-contact atomic force microscopy (nc-AFM) measurements⁶ have confirmed that the negative to neutral charge transition of isolated dangling bonds occurs at energies on the order of approximately 300 meV below the bulk Fermi level. This enables their charge state to be selectively modified by shifting this charge transition level above or below the bulk Fermi level. By performing a series of nc-AFM experiments we study and control the charge states of the engineered atomic structures with single

electron charge sensitivity. All experiments are performed with no applied bias between the tip and sample. With the tip-sample separation as our key experimental parameter we uncover two interaction regimes: a strongly interacting regime where we can controllably position single electrons within the structures; and a weakly interacting regime, approximating field-free conditions, where we can non-perturbatively track the position of charge within the structures over time.

In Fig. 1, two dangling bonds are patterned with two intervening hydrogen atoms using hydrogen lithography¹⁶. Figure 1a and 1b display filled and empty states scanning tunneling microscope (STM) images of the pair. In a constant height frequency shift (Δf) image of this structure (zero bias, Fig. 1c) the dangling bonds appear dark due to additional Coulombic attraction. Two closely-spaced negatively charged dangling bonds experience Coulombic repulsion great enough that one electron is ejected to the conduction band. Consequently, images of the pair appear streaky, as the single remaining negative charge is shared between the pair, switching sites multiple times over the time it takes to acquire an image. This is seen clearly in individual Δf line scans across the structure (Fig. 1d) which reveal the localization of charge to one dangling bond, with subsequent line scans demonstrating that this charge occasionally switches to the other dangling bond.

Changes in the distribution of charge within the pair can be followed over time by stacking sequential Δf line scans (Fig. 1e). Previous theoretical estimates for the tunneling rate between two closely-spaced dangling bonds have ranged from THz to GHz, depending on the spacing²³. Surprisingly, the bistable signal for each dangling bond extracted from Fig. 1e demonstrates that the charge states often remain trapped for seconds (Fig. 1f), indicating that elastic tunneling between the paired atoms is not occurring. Recent studies have revealed that charged species are often stabilized by a lattice relaxation of the supporting substrate^{9,24}. Density functional theory has similarly shown that negatively charged silicon dangling bonds experience approximately 200 meV stabilization due to a relaxation of the lattice which raises the nuclear position of the host atom by approximately 30 pm^{23,25}, which in this case prevents elastic tunneling of the electrons between neighboring dangling bonds. To reliably assign the position of the charge in each Δf line scan, the two dangling bond-centered features were fit with Gaussian profiles. Histograms of the determined Δf show two well-separated maxima, which can be reliably assigned to the negative and neutral charge states of each dangling bond (Fig. 1g and Supporting Information Fig. S1 and Fig. S3). This permits a binary number to be assigned to the charge configuration in each line scan.

We noticed that the occupation of the structure appeared to depend on tip-sample spacing, motivating further study. We performed a series of constant height line scan maps on a symmetric

structure composed of six dangling bonds (Fig. 2a-d), each with different tip-sample separations. The average occupation of each dangling bond at each height can be inferred from histograms of the Δf measured over each dangling bond (Supporting Information, Fig. S3). More simply, the average occupation of the entire structure can be inferred by counting the number of dark bars in each line scan map, which is observed to decrease as the tip-sample separation is increased (Fig. 2e).

To understand this trend we modelled the interaction between the tip and dangling bonds with a 3D finite-element numerical model^{26,27}, which reveals the height-dependence of the band bending beneath the tip (Fig. 3a). Two contributions to the total tip induced band bending (TIBB) at zero bias must be considered: (i) the contact potential difference between the tip and substrate; (ii) a contribution by the image charge induced in the AFM tip. Because the work function of our tungsten tip is ~ 1 eV greater than that of the substrate the contact potential difference results in an upward band bending contribution to the surface. When the DB is negative, the image charge induced in the tip produces a counteracting contribution, which has an approximate $1/z$ dependence on tip height (z). At small tip-sample separations, the effect of the image charge can exceed that of the contact potential difference, rendering the total potential energy negative. Under these conditions, an electron is stabilized in the dangling bond directly beneath the tip (for simulation details see Supplementary Information, Fig. S2) permitting the tip to be used as a means to manipulate electrons confined to the atomic structure. This effect vanishes with increasing tip-sample separation (Fig. 2f). Furthermore, as the tip is retracted the true occupation of the structure is observed (Fig. 2e). In this regime, the charge configuration of the system appears to remain unchanged for many measurements (>15 s on average for both states), suggesting that the tip is nearly non-interacting with the system. From this we conclude that there are two interaction regimes (Fig. 2e): a strongly interacting regime with small tip-sample separations where the charge is controllably manipulated by the tip (the *write* regime), and a weakly interacting regime where we can observe the natural charge occupation of the structure (the *read* regime).

Analysis of the charge states observed in the *read* regime can be used to infer their relative energies. Inspection of Fig. 2d reveals that the outermost dangling bonds are continuously charged, however, only a single negative charge is electrostatically confined to the interior of the structure, where it occasionally switches between the two central dangling bonds. By observing that the total amount of time the central charge spends in the left dangling bond (50%) is roughly equal to the right (46%), we confirm the degeneracy of these two charge states.

To further validate our assignment of the *write* and *read* regimes we performed the experiments depicted in schemes Fig. 3a-c on the symmetric structure (Fig. 3d, the same structure as in Fig. 2) and an asymmetric structure (Fig. 3i). First, we restricted the measurements to the *read* regime (scheme Fig. 3a, Fig. 3e,j), allowing us to characterize the intrinsic charge states of the structures and assess their relative energies based on their rate of occurrence (Fig. 3h,m). Subsequent experiments contain two associated phases: in the *write* phase, the tip is scanned across the structure at close proximity; in the *read* phase, the tip is retracted 50 pm with respect to the *write* phase and scanned back across (depicted in schemes Fig. 3b,c). It might be expected that any charge state prepared by the *write* phase should be observed in the *read* phase. Indeed, Fig. 3f,g and 3k,l confirm that charge in the interior of both structures can be manipulated. On the symmetric structure (Fig. 3d) we could consistently initiate charge to the right (Fig. 3f, 85%) or left (Fig. 3g, 79%) central dangling bond, corresponding to preparation of the degenerate ground states observed in Fig. 3e and Fig. 2d. On the asymmetric structure (Fig. 3i), measurements restricted to the *read* regime (Fig. 3j) demonstrate that this system has three negative charges, again only the charge confined to the inner pair fluctuates, and because the structure is asymmetric these two charge states are non-degenerate. Although we expected this charge to favor the left dangling bond of the pair we observe the opposite (Fig. 3j,m 18% vs. 73%, respectively). This indicates that other charged species (*e.g.* dangling bonds or ionized donors) act as an additional electrostatic bias on this structure, however, these hidden biases can be counteracted by patterning additional dangling bonds in the structure's surrounding area (Supporting Information, Fig. S5). Using the techniques previously described the central charge could be manipulated to selectively occupy the right (Fig. 4j, 92%) or left (Fig. 4k, 67%) dangling bond of the pair, corresponding to the ground and excited states observed to occur in Fig. 3j, respectively. These results demonstrate that ground states can be prepared with high efficiency and the occurrence rate of excited charge states can be strongly enhanced. We note that the charge in the right-hand pair of the asymmetric structure could not be manipulated. We hypothesize this is because the other two charges in the structure act as strong electrostatic biases, and that to observe the excited charge states corresponding to its manipulation would require greater time resolution than was available to us (~1s between *write* and *read* phases).

These results demonstrate that charge states in atomic structures can remain trapped for periods on the order of seconds. This is because dangling bonds are electronically isolated from the bulk and lattice relaxation induces an asymmetry in the confining potential. As a result, thermal fluctuations are required to provide the activation energy required for electrons to tunnel or thermionically hop between dangling bonds. This motivates a temperature-dependent study of these phenomena. Our results can be

interpreted *via* electrostatic arguments suggesting atomic systems could serve well as the building blocks for field controlled computing devices. We identify the height dependence of tip induced band bending in AFM experiments at zero bias as the key factor to manipulate and non-perturbatively monitor single-electrons confined to atomic structures. The techniques presented here expand the scanning probe toolkit with the ability to position charge within atomic structures and initiate desired charge states, opening the door for future investigations of tailor-made atomic charge configurations and hardware systems modelling designer Hamiltonians.

Methods

Experimental Setup: All experiments were performed on a home built system incorporating an Omicron LT STM/AFM operating at 4.5 K and ultrahigh vacuum ($< 1 \times 10^{-10}$ Torr). The tip was created from polycrystalline tungsten wire that was chemically etched and installed to a qPlus sensor²⁸. The tip was driven with an amplitude of 50 pm at a resonance frequency of 28 kHz and Q-factor of 14×10^3 . An additional electrode on the sensor is used to supply tunneling current. Tips were further processed with electron bombardment to remove the surface oxide, and sharpened by nitrogen etching while performing field ion microscopy²⁹. *In-situ* tip processing was performed by controlled contacts with the tip to the sample surface. Samples were cleaved from (100)-oriented Si crystals that are highly As-doped (1.5×10^{19} atom cm^{-3}). After degassing at 600 °C for ~12 hours, samples were flash annealed to temperatures as high as 1250 °C before passivating the surface with hydrogen while maintaining a sample temperature of 330 °C. These high flash temperatures have been previously shown to induce a dopant depletion region extending as far as 100 nm below the sample surface^{30,31}.

Acknowledgements

We would like to thank Mark Salomons and Martin Cloutier for their technical expertise. We also thank Leo Gross and Gerhard Meyer for stimulating discussions. We thank NRC, NSERC, and AITF for their financial support.

Author contributions

M.R., W.V., J.R., K.W., and R.W. conceived the experiments. M.R. and T.D. performed the experiments with input from T.H. and W.V.. W.V. analyzed the data. W.V., M.R. and T.D. prepared the manuscript. L.L. developed the model of the interaction between tip and surface. All authors reviewed and commented on the manuscript.

Competing Financial Interest:

A patent has been filed on this subject. Some of the authors are affiliated with Quantum Silicon Inc (QSi). QSi is seeking to commercialize atomic silicon quantum dot based technologies.

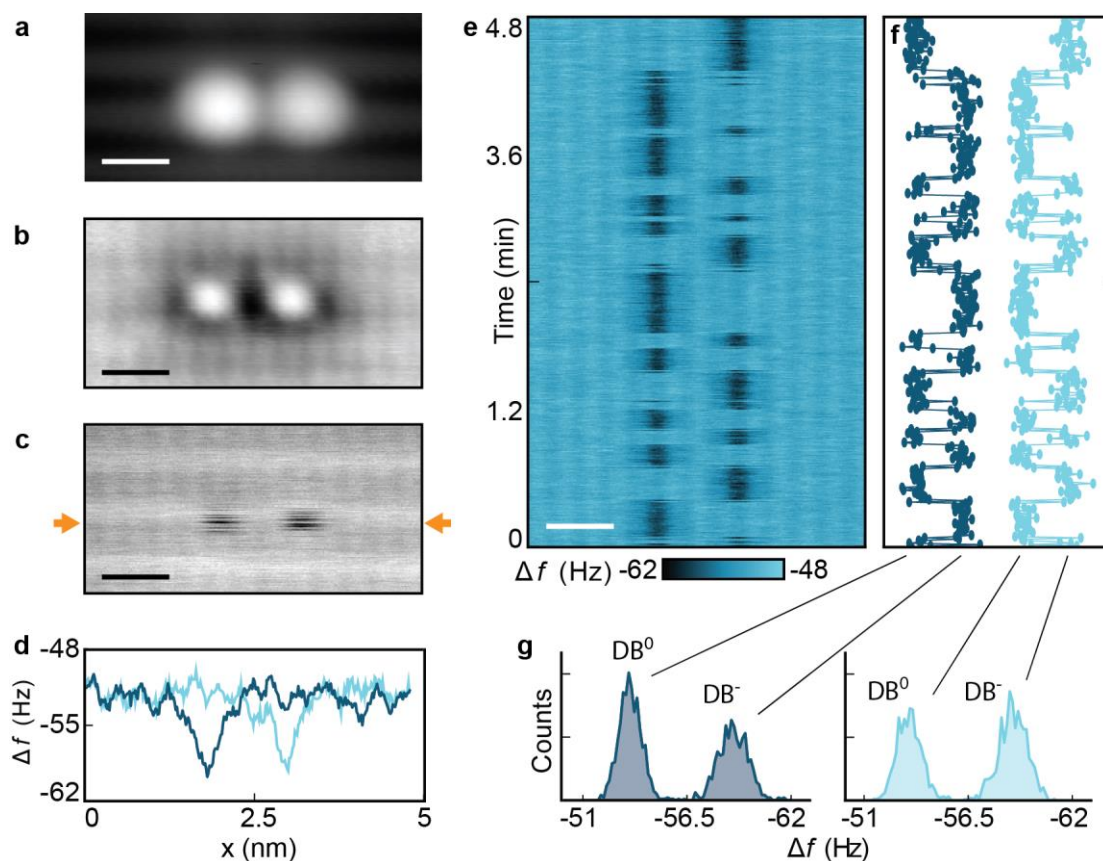


Figure 1: Fluctuating charge states of two closely-spaced dangling bonds (DB). (a) Constant current filled state STM image of the structure recorded at -1.8V and 50 pA. (b) Constant current empty state STM image recorded at 1.3 V and 50 pA. (c) Constant height Δf image of the structure taken at 0 V. The initial tip height is set on a hydrogen atom at -1.8 V and 50 pA before moving the tip 300 pm towards the surface (d) Two individual line scans made in constant height AFM mode along a line indicated by the orange arrows in (c) with a tip offset of -300 pm from the setpoint and at 0 V. The change of peak position is attributed to the electron jumping from one side of the DB pair to the other. (e) Combined map of 400 constant height Δf line scans taken sequentially over a five minute period. (f) Time-dependent bistable signal for the two individual DBs. (g) Histograms extracted from the signals in (f). Labels indicate the charge state assignment of each peak. Scale bar is 1 nm (a-c, e).

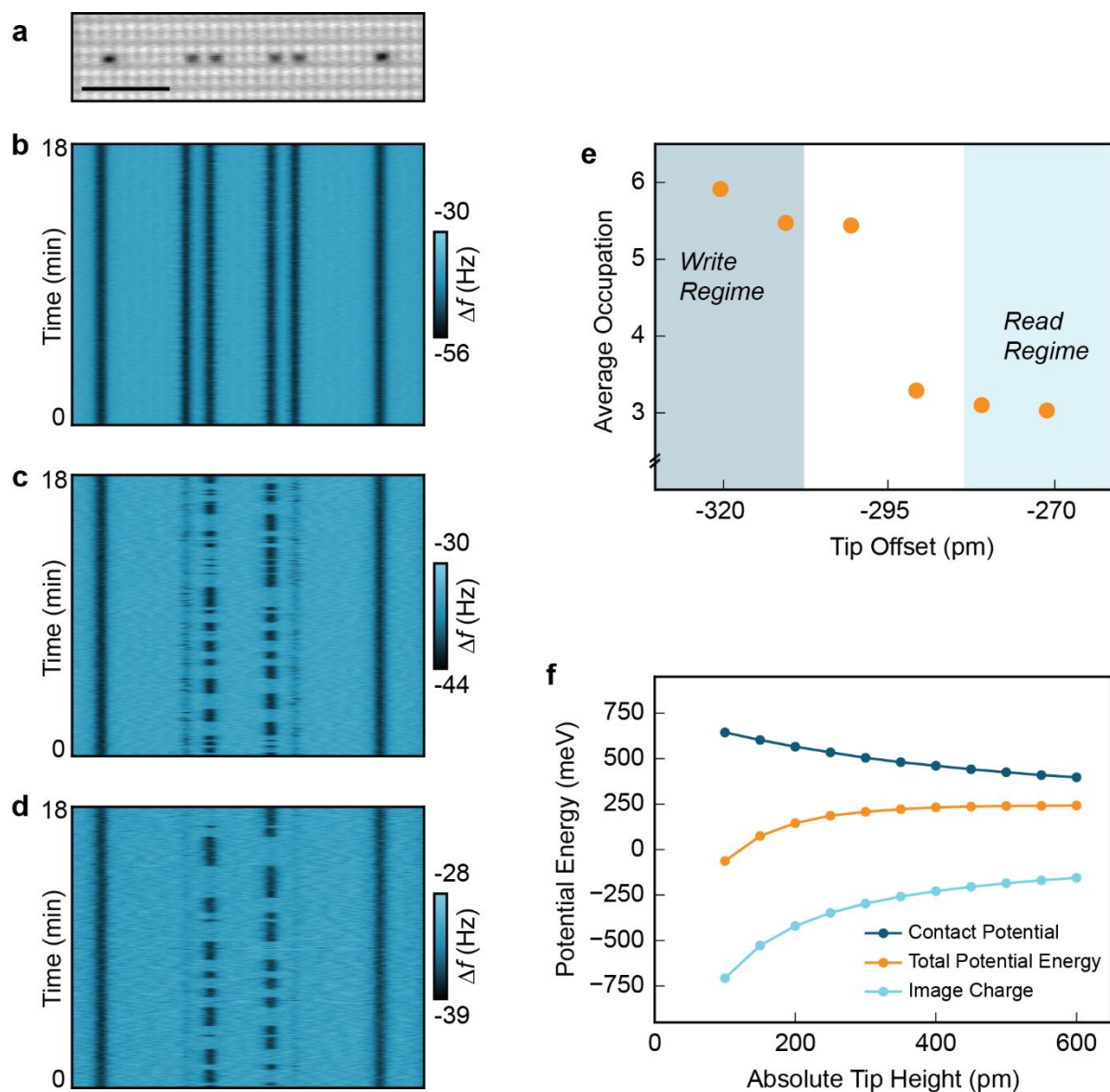


Figure 2: Charge state evolution of a symmetric six dangling bond structure at different tip heights. (a) Constant height Δf image of the symmetric six dangling bond structure taken at -300 pm and 0 V. The scale bar (a-d) is 3 nm. (b-d) Eight hundred constant height line scans at -320 pm (b), -290 pm, (c) and -270 pm (d) reveal the evolution of the system's charge states in time. Tip heights are in reference to an STM setpoint of -1.8 V and 50 pA measured over H-Si. Images contain sweeps in both directions across the sample. Histograms of the Δf extracted over each dangling bond in (b) and (d) are available in Supplementary Information Fig. S4. (e) The average occupation of the structure, inferred from digitizing the charge state of 1600 constant height Δf line scans at different tip offsets, decreases from six to three negative charges as the tip sample separation is increased. Two interaction regimes: *read* and *write* are indicated. (f) Modelling of the total tip-induced potential energy of the DB electron as sum of two components at zero bias: the contact potential difference between tip and sample and the image charge induced in the AFM tip. The tungsten AFM tip was assumed to have a work function of 5 eV and an apex radius of 5 nm as observed during field ion microscope imaging of tip. The sample's work function was taken to be 4.1 eV. Additional modelling information is available in Supplementary Information.

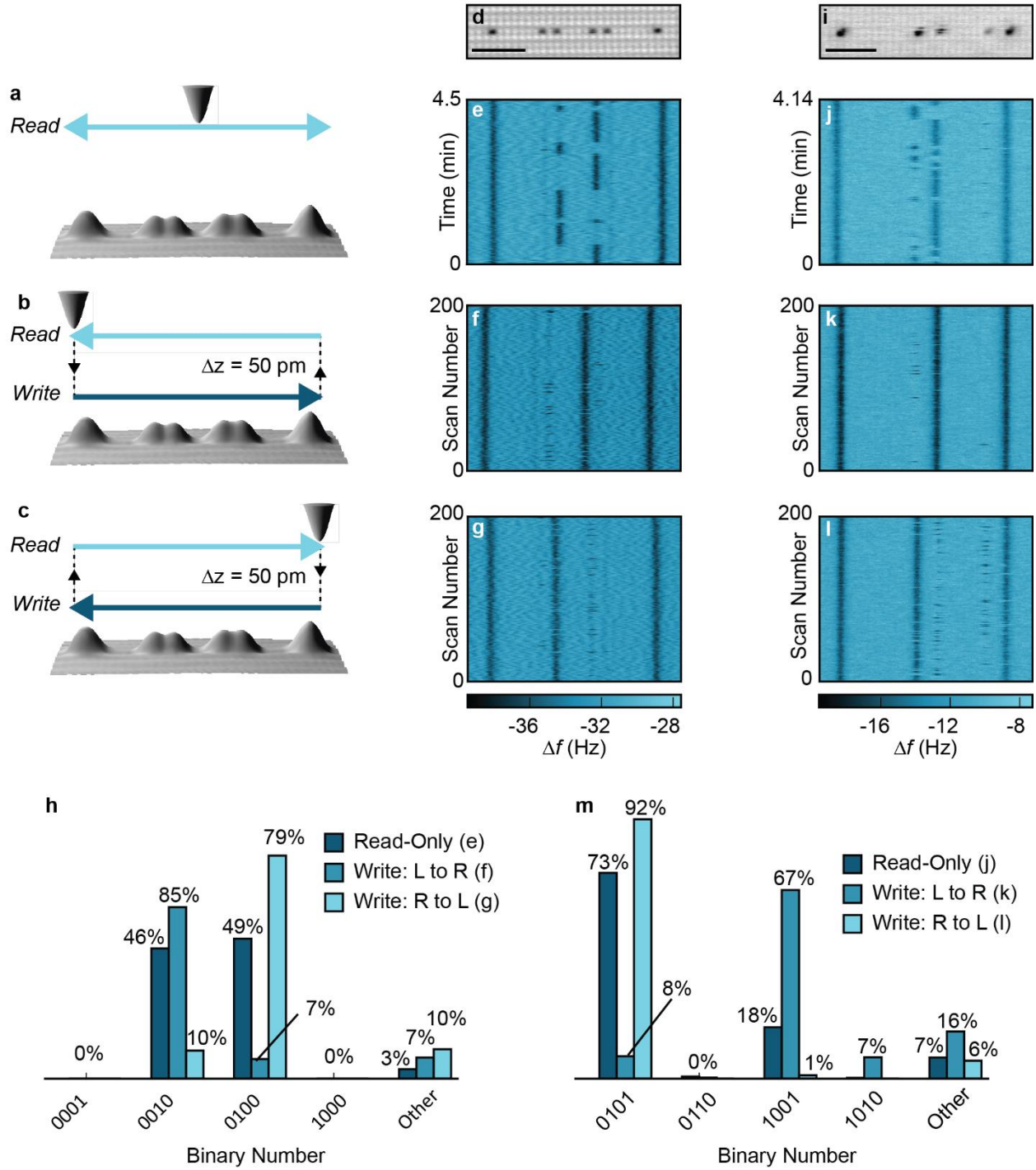


Figure 3: Controlled preparation of charge states in symmetric and asymmetric dangling bond structures. Visualization of the scan modes: **(a)** all measurements are restricted to the *read* regime; **(b)** The tip is scanned from left to right in the *write* regime, retracted 50 pm to the *read* regime, and scanned back across; **(c)** the same process as **(b)** with directions reversed. **(d)** Constant height Δf image of the symmetric six-dangling bond structure taken at -300 pm and 0 V. **(e-g)** 200 line scans across structure in **(d)** corresponding to scheme **(a)** **(e)**, scheme **(b)** **(f)**, and scheme **(c)** **(g)** (*write* regime: -320 pm, *read* regime: -270 pm). **(h)** Histograms of the binary numbers determined from digitization of the line scans in **(e-g)**. 0's and 1's correspond to neutral and negatively charged dangling bonds,

respectively. Only the four interior dangling bonds are considered. (i) Constant height Δf image of the asymmetric five-dangling bond structure taken at -350 pm and 0 V. (j-l) Maps of 200 line scans across structure (i) corresponding to scheme (a) (j), scheme (b) (k), and scheme (c) (l) (write regime: -370 pm, read regime: -320 pm). (m) Histograms of the binary numbers determined from digitization of the line scans in (j-l). The scale bars in (d) and (i) are 3 nm. Tip heights are in reference to an STM constant current setpoint of -1.8 V and 50 pA measured over H-Si.

References

1. Schweizer, D. K. & Eigler, E. K. Positioning single atoms with a scanning tunneling microscope. *Nature* **344**, 524–525 (1990).
2. Sugimoto, Y. *et al.* Complex Patterning by Vertical Interchange Atom Manipulation Using Atomic Force Microscopy. *Science* **322**, 413–417 (2008).
3. Slot, M. R. *et al.* Experimental realization and characterization of an electronic Lieb lattice. *Nat. Phys.* **13**, 672–676 (2017).
4. Drost, R., Ojanen, T., Harju, A. & Liljeroth, P. Topological states in engineered atomic lattices. *Nat. Phys.* **13**, 668–671 (2017).
5. Fölsch, S., Martínez-Blanco, J., Yang, J., Kanisawa, K. & Erwin, S. C. Quantum dots with single-atom precision. *Nat. Nanotechnol.* **9**, 505–508 (2014).
6. Huff, T. *et al.* Binary Atomic Silicon Logic. *arXiv:1706.07427* (2017).
7. Fuechsle, M. *et al.* A single-atom transistor. *Nat. Nanotechnol.* **7**, 242–246 (2012).
8. Kalff, F. E. *et al.* A kilobyte rewritable atomic memory. *Nat. Nanotechnol.* **11**, 926–929 (2016).
9. Repp, J., Meyer, G., Olsson, F. E. & Persson, M. Controlling the Charge State of Individual Gold Adatoms. *Science* **305**, 493–495 (2004).
10. Gross, L. *et al.* Measuring the Charge State of an Adatom with Noncontact Atomic Force Microscopy. *Science* **324**, 1428–1431 (2009).
11. Steurer, W. *et al.* Manipulation of the Charge State of Single Au Atoms on Insulating Multilayer Films. *Phys. Rev. Lett.* **114**, 36801 (2015).
12. Sterrer, M. *et al.* Control of the charge state of metal atoms on thin MgO films. *Phys. Rev. Lett.* **98**, 96107 (2007).
13. Leoni, T. *et al.* Controlling the charge state of a single redox molecular switch. *Phys. Rev. Lett.* **106**, 216103 (2011).
14. Steurer, W., Fatayer, S., Gross, L. & Meyer, G. Probe-based measurement of lateral single-electron transfer between individual molecules. *Nat. Commun.* **6**, 8353 (2015).
15. Bennett, S. D., Cockins, L., Miyahara, Y., Grutter, P. & Clerk, A. A. Strong electromechanical coupling of an atomic force microscope cantilever to a quantum dot. *Phys. Rev. Lett.* **104**, 17203 (2010).

16. Lyding, J. W., Shen, T., Hubacek, J. S., Tucker, J. R. & Abeln, G. C. Nanoscale patterning and oxidation of H-passivated Si(100)-2×1 surfaces with an ultrahigh vacuum scanning tunneling microscope. *Cit. Appl. Phys. Lett. J. Chem. Phys* **64**, 2010–2012 (1994).
17. Rashidi, M. *et al.* Time-Resolved Imaging of Negative Differential Resistance on the Atomic Scale. *Phys. Rev. Lett.* **117**, 276805 (2016).
18. Liu, L., Dienel, T., Widmer, R. & Gröning, O. Interplay between Energy-Level Position and Charging Effect of Manganese Phthalocyanines on an Atomically Thin Insulator. *ACS Nano* **9**, 10125–10132 (2015).
19. Schulz, F. *et al.* Many-body transitions in a single molecule visualized by scanning tunnelling microscopy. *Nat. Phys.* **11**, 229–234 (2015).
20. Huff, T. R. *et al.* Atomic White-Out: Enabling Atomic Circuitry through Mechanically Induced Bonding of Single Hydrogen Atoms to a Silicon Surface. *ACS Nano* **11**, 8636–8642 (2017).
21. Pavliček, N., Majzik, Z., Meyer, G. & Gross, L. Tip-induced passivation of dangling bonds on hydrogenated Si(100)-2 × 1. *Appl. Phys. Lett.* **111**, 53104 (2017).
22. Jarvis, S., Sweetman, A., Bamidele, J., Kantorovich, L. & Moriarty, P. Role of orbital overlap in atomic manipulation. *Phys. Rev. B* **85**, 235305 (2012).
23. Livadaru, L. *et al.* Dangling-bond charge qubit on a silicon surface. *New J. Phys.* **12**, 83018 (2010).
24. Olsson, F. E., Paavilainen, S., Persson, M., Repp, J. & Meyer, G. Multiple charge states of Ag atoms on ultrathin NaCl films. *Phys. Rev. Lett.* **98**, 176803 (2007).
25. Schofield, S. R. *et al.* Quantum engineering at the silicon surface using dangling bonds. *Nat. Commun.* **4**, 1649 (2013).
26. Livadaru, L., Pitters, J., Taucer, M. & Wolkow, R. A. Theory of nonequilibrium single-electron dynamics in STM imaging of dangling bonds on a hydrogenated silicon surface. *Phys. Rev. B* **84**, 205416 (2011).
27. Feenstra, R. M. Electrostatic potential for a hyperbolic probe tip near a semiconductor. *J. Vac. Sci. Technol. B* **21**, 2080 (2003).
28. Giessibl, F. J. Atomic resolution on Si(111)-(7×7) by noncontact atomic force microscopy with a force sensor based on a quartz tuning fork. *Appl. Phys. Lett.* **76**, 1470–1472 (2000).
29. Rezeq, M., Pitters, J. & Wolkow, R. Tungsten nanotip fabrication by spatially controlled field-assisted reaction with nitrogen. *J. Chem. Phys.* **124**, 204716 (2006).
30. Rashidi, M. *et al.* Time-resolved single dopant charge dynamics in silicon. *Nat. Commun.* **7**, 13258 (2016).
31. Pitters, J. L., Piva, P. G. & Wolkow, R. A. Dopant depletion in the near surface region of thermally prepared silicon (100) in UHV. *J. Vac. Sci. Technol. B* **30**, 21806 (2012).

Supplementary Information:

Initiating and monitoring the evolution of single electrons within atom-defined structures

Mohammad Rashidi^{1,2,3*}, Wyatt Vine^{1*}, Thomas Dienel^{1,2*}, Lucian Livadaru³, Jacob Retallick⁴, Taleana Huff^{1,3}, Konrad Walus⁴, Robert A. Wolkow^{1,2,3}

¹Department of Physics, University of Alberta, Edmonton, AB, Canada, T6G 2R3

²Nanotechnology Initiative, Edmonton, AB, Canada, T6G 2M9

³Quantum Silicon, Edmonton, AB, Canada, T6G 2M9

⁴Department of Electrical and Computer Engineering, University of British Columbia, Vancouver, BC, Canada, V6T 1Z4

*Authors contributed equally

Correspondence to: rashidi@ualberta.net, wyattvine@gmail.com, thdienel@gmail.com

Table of Contents:

- Definition and discussion of error rate
- Description of data processing and assignment of binary number
- Modeling and potential energy of dangling bonds during AFM imaging
- Additional experimental data

Error Rate: Throughout measurements restricted to the *read*-regime we occasionally observed negative charges occupying both dangling bonds in a pair, despite this being unlikely due to Coulombic repulsion. We define these line scans as errors. While it was typically several percent we have achieved error rates of <1% (Supporting Information, Fig. S2). We have identified several contributing factors. (i) The *read* and *write* regimes are sensitive to the tip height (Fig. 3). Accordingly, we find that small changes in tip height can occasionally result in unintentional dragging in the *read*-regime causing the same negative charge to be measured twice, or influence our ability to control the negative charge in the *write*-regime. (ii) Sharp tips were found to more clearly resolve the two charge states of each dangling bond. This reduces the number of incorrect charge state assignments, which are performed in a digital fashion. Similarly, with H-terminated tips, which can be effectively identified via force distance spectroscopy²⁴, it was more difficult to discriminate the two charge states each dangling bonds.

Data Processing: Minimal data processing was performed, and raw data was used whenever possible. All experiments with repeated line scans were performed in constant height mode. For experiments performed entirely in the *read* regime, forward and backward line scans, which are saved in separate files by the control software, were aligned manually by removing an equal number of pixels at the start of both scans and zipped together (step 1, Fig. S1b). Measurements often exceeded 30 minutes, over which time the tip would inevitably drift towards or away from the surface due to piezo creep and thermal drift. To

account for this, a linear drift was subtracted from all measurements with repeated line scans by fitting the average Δf for each line scan over the course of an experiment (step 2, Fig. S1c). In experiments where Δf drifted by more than 2 Hz the entire run was rejected.

The Δf value measured over each dangling bond was extracted by independently fitting each dangling bond associated peak in the line scans (defined by pixels) with a Gaussian function (step 3, Fig. S1d). When dangling bonds were neutral, this corresponded to fitting the Δf associated with the background noise/hydrogen, and therefore the peak of each Gaussian was constrained to a 30-pixel window centered on each dangling bond. Supporting Figure S1e,f shows the extracted Δf values for two dangling bonds. The bistable behavior of each dangling bond is clearly visible.

Binary numbers were assigned to the charge states by making a single cut in Δf (Fig. S1e,f demonstrate cuts). Dangling bonds with Δf more negative than the cut (larger absolute Δf) were assigned a negative charge state, while those with Δf more positive than the cut (smaller absolute Δf) were assigned a neutral charge state (Fig. S1e,f). Two additional steps were used to create the histograms in Fig. S3 and S4. First, the largest Δf in the set of the Δf extracted for all the dangling bonds in an experiment (corresponding to a fit of the background) was set to 0 (step 4). Thus, the normalized Δf for all the dangling bonds would be positive. Second, each Δf was normalized by setting the average Δf for the two isolated dangling bonds to 1.0 (step 5). Because the isolated dangling bonds were always negatively charged, a normalized Δf of 1.0 corresponds to the average Δf for a negatively charged dangling bond. Similar to the process above a single common cut in Δf was used to assign charge states to the normalized data (step 6).

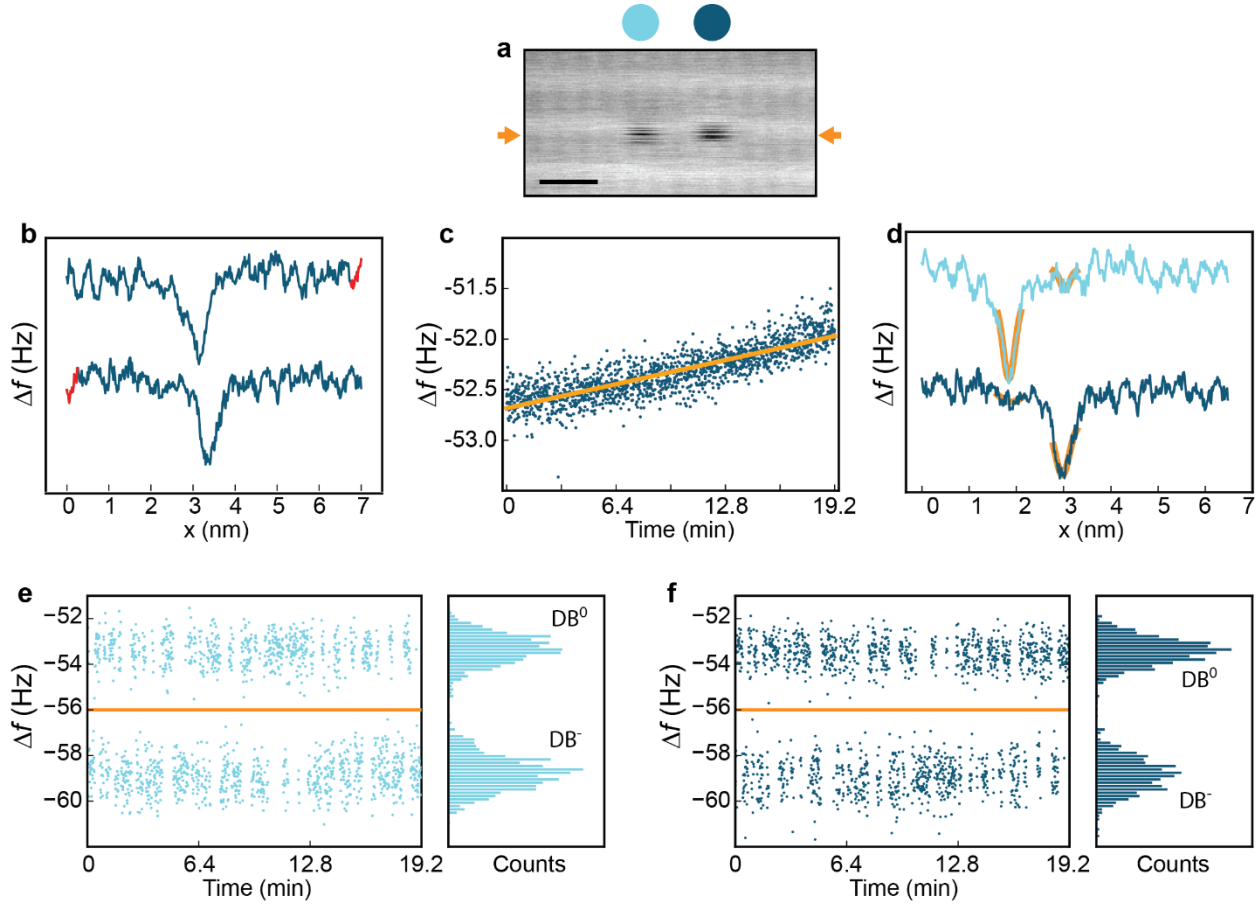


Figure S1: Illustration of data processing routine. (a) Constant height Δf image of a dangling bond structure taken at 0 V. The initial tip height is set on a hydrogen atom at -1.8 V and 50 pA before moving the tip 300 pm towards the surface. The scale bar is 1 nm. (b) Two sequential Δf line scans demonstrate negative charge confined to the right-hand dangling bond (line scan width is larger than the window shown in (a), line scans are offset for clarity). The peaks are not aligned because they correspond to forward (top) and backward (bottom) line scans, which typically have a fixed offset due to piezo creep. The red tails on both line scans demonstrate the data that is chopped to align the scans. (c) The average Δf of each line scan over the course of the entire experiment demonstrates that the tip was slowly drifting away from the sample. A linear fit of this data (orange line) is subtracted from the dataset. (d) Each line scan is fit with two gaussian peaks to extract the Δf over each dangling bond (colour legend indicated above (a)). Note that for neutral dangling bonds this corresponds to a fit of the signal associated with hydrogen/noise. (e-f) The Δf extracted for each dangling bond clearly displays two distinct states, which we assign to the negative and neutral charge states of each dangling bond. Each histogram has 75 equal width bins between $\Delta f = -62$ and -51 Hz, and has an integrated area of 1.0.

Potential energy of DBs during AFM imaging: The eigenenergies of a single DB in neutral and negative states are estimated to be $E(DB^-) = -320$ meV and $E(DB^0) = -770$ meV with respect to the bulk conduction band maximum (CBM) at flat band conditions⁵. The valence band minimum (VBM) in silicon is -1.17 eV with respect to the CBM at temperatures close to 0 K. We therefore identify the ways in which the tip contributes to the potential energy of DBs during non-contact AFM imaging at zero bias: (i) a shift in energy landscape due to the tip-sample contact potential, known as tip-induced band bending (TIBB) and (ii) an image charge contribution to the potential energy, dubbed image-charge-induced band bending

(ICIBB). The AFM tip was assumed to have a work function of 5 eV and an apex radius of 5 nm while the sample work function was taken to be 4.1 eV. A 3D finite-element Poisson equation solver was employed to calculate TIBB⁶. The image charge was calculated using a dielectric constant of 6.35, equal to the average of vacuum and silicon dielectric constants because the lobes of the dangling bonds extend into both mediums. The results are summarized in Fig. 2f in the main manuscript, showing the two energy components at zero bias as a function of tip height. The numerical results in Fig. 2f show that the TIBB (contribution of contact potential difference between the tip and the sample) is upward and is counteracted by the image charge component, which remarkably has an approximately $1/z$ dependence on tip height z and becomes very important at small tip-sample separations where it can locally exceed TIBB, thus rendering the total potential energy felt by the electron to be negative. Therefore, the electron on a negative dangling bond can be greatly stabilized by the ICIBB as depicted in Fig. S2a. As a result, these combined energy shifts render the level of the single negative dangling bond state lower than the Fermi level of the tip by about 170 meV and, as the tip is within the tunneling range of the dangling bond, the latter acquires a net negative charge. However, as tip height is increased, the total potential energy of the DB electron increases (even though TIBB decreases) to the point where the DB⁻ state is brought above the tip Fermi level and the localized DB electron tunnels into the tip rendering the DB neutral. As a side note: the effect of coating the AFM tip with silicon material (as some reports have indicated occurs due to *in-situ* tip preparation via controlled contacts with the surface) results in a lower work function of the tip, and therefore a reduced TIBB. It also decreases the image charge potential by increasing the effective separation between the metal and the dangling bond charge center.

However, when a few dangling bonds are assembled in a system such as those in Fig. 2 and Fig. 4, their charging states become selective according to the mutual repulsion among them in order to minimize the total energy of the system. For example, in experiments conducted in the *read* regime, excessive Coulomb repulsion between two close dangling bonds (0, 1, or 2 H atoms apart) prohibits equal charging of these dangling bonds, and only one extra electron is allowed in such a pair. This situation is depicted in Fig. S2b where two dangling bonds are assumed to be separated by one H atom, as are the two dangling bond pairs in Fig. 2 of the main text. If one of the two dangling bonds were negatively charged, the repulsion energy at the site of the other dangling bond (which we dub the perturber-induced band bending, PIBB) amounts to ~280 meV, as calculated by simple electrostatics using point charges and a dielectric constant of the surface of 6.35. In addition to this, the PIBB from the far dangling bonds increase the potential energy of middle dangling bonds even more by a few tens of meV. This brings the total potential energy at that site to above the Fermi level by about 100 meV, leaving that dangling bond neutral. Note that, importantly, in the *write* regime the ICIBB can increase in magnitude by more than 100 meV if the tip height is below 200 pm (Fig. 2f). This has the effect of bringing the negatively charged dangling bond level below the Fermi level of the tip and both dangling bonds are seen to harbor a negative charge during this phase (Fig. 2b).

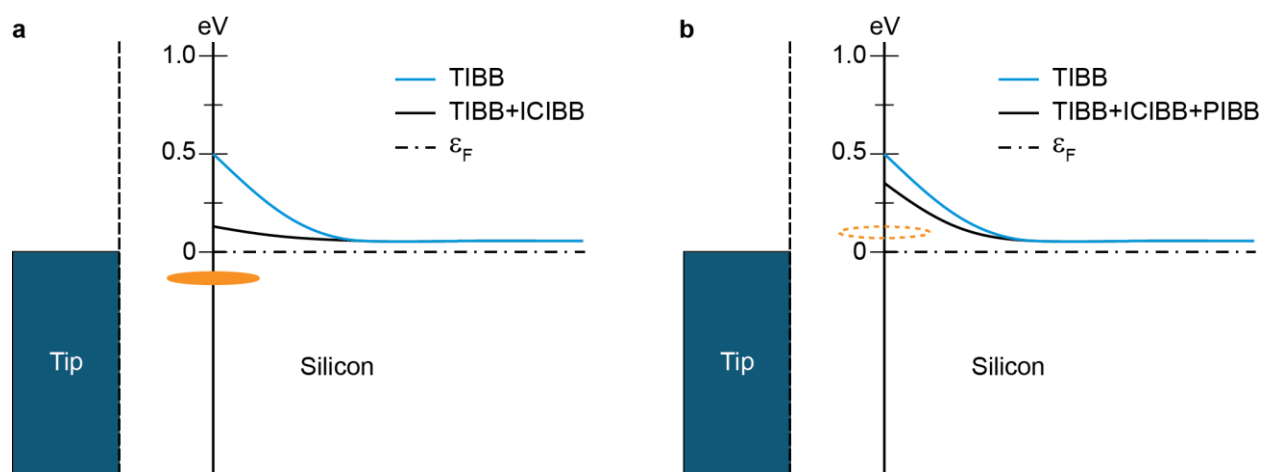


Figure S2: Potential energy diagram for an isolated dangling bond at zero bias and with a small tip-sample separation. (a) At small tip height, the electron is stabilized on a DB by the effect of the ICIBB counteracting the TIBB, such that the level of the DB⁻ state (filled green oval) is lower than the Fermi level of the tip (upper edge of the blue rectangle) and thus is stably occupied. The graph also shows potential energy variations (band bending) as a function of sample depth (horizontal axis), where the dash-dotted line is the sample Fermi level and the solid curves represent the CBM. (b) If a DB is located near some other DB, already negative, there is another component (PIBB) to the total potential energy coming from the Coulomb repulsion. This renders the total energy of the DB⁻ level (empty red oval) above the Fermi level of the tip and the sample, therefore keeping that DB neutral.

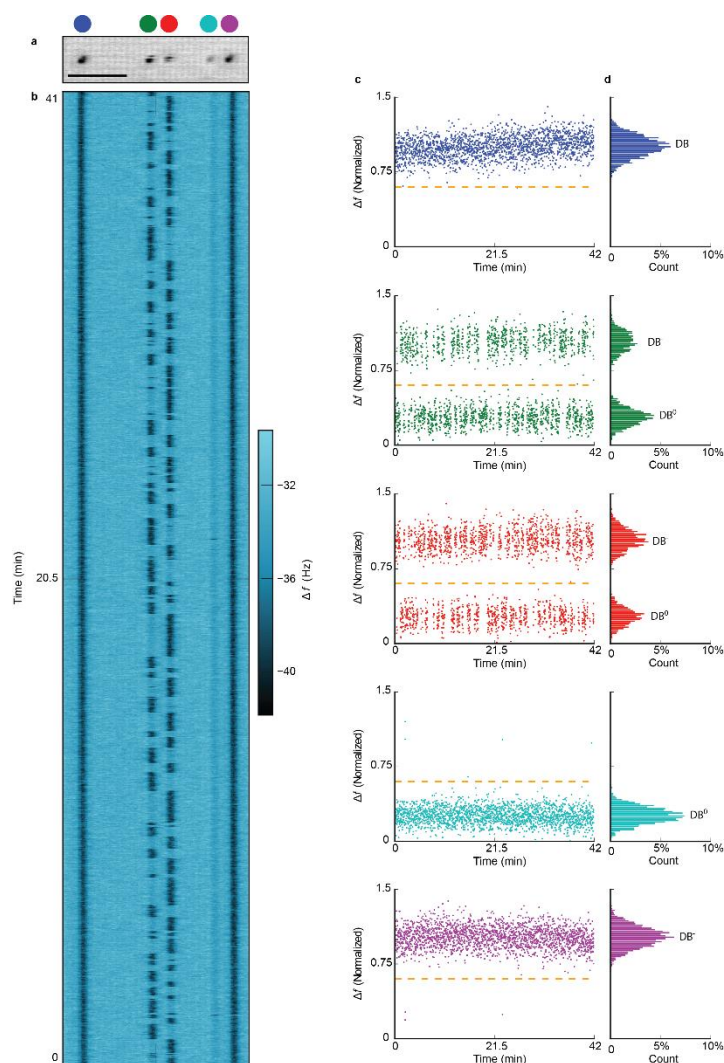


Figure S3: Digitization of line scans of an asymmetric structure composed of five dangling bonds. (a) Constant height Δf image of the dangling bond structure at 0 V. (b) A line scan map composed of 2048 Δf line scans acquired in the *read*-regime (-300 pm) over structure demonstrate. (c) The normalized Δf acquired over each dangling bond throughout the course of the experiment demonstrates clearly that there are two charge states of each dangling bond (although only the green and red dangling bonds appear to fluctuate between them). With the normalizing procedure described above the negative dangling bond charge state is normalized to a Δf of 1.0, and the Δf of the neutral dangling bond state is centered approximately at 0.25. The orange dotted lines demonstrate that a single common cut of $\Delta f = 0.6$ in the normalized data can be used to digitize the charge state of the structure with each line scan. (d) Histograms of the normalized Δf for each dangling bond reveal that the Δf corresponding to the two charge states of each dangling bond have a Gaussian distribution. Upon assigning binary numbers to this dataset it was found that in <1% of the line scans the charge configuration corresponded to having a third negative charge in the four paired dangling bonds. Each histogram has 75 equal width bins between $\Delta f(\text{normalized}) = 0$ and 1.5, and has an integrated area of 1.0.

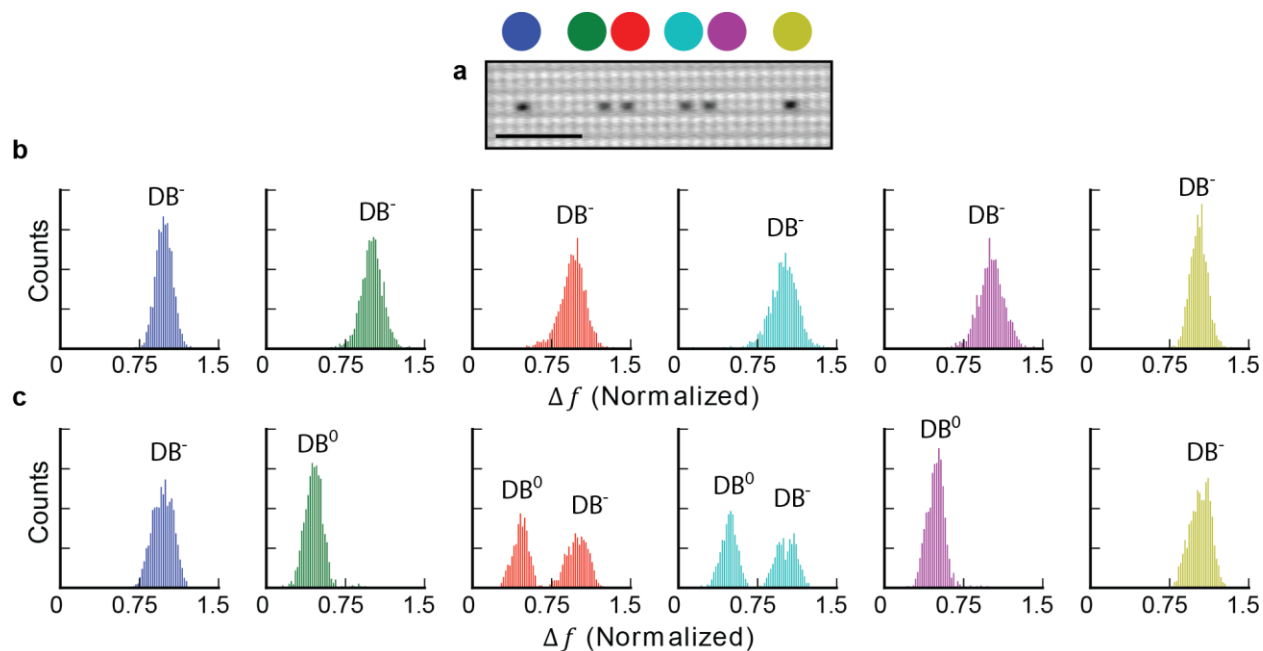


Figure S4: Histograms of the normalized Δf measured over each site in a symmetric six dangling bond structure at different tip heights. (a) Constant height Δf image of the structure. Histograms of the normalized Δf measured over each dangling bond at (b) $z = -320$ pm and (c) $z = -270$ pm. 1600 line scans at both heights were used to gather statistics. Each histogram has 75 equal width bins between $\Delta f(\text{normalized}) = 0$ and 1.5, and has an integrated area of 1.0. All the dangling bonds appear negatively charged in (b). In (c), the isolated dangling bonds on either end (blue and yellow) remain negatively charged while the outer atoms of each pair (green and purple) are neutral. In (c) the inner atoms (red and cyan) fluctuate between the neutral and negative charge states; the integrated area of each peak is approximately 0.5, indicating they are equally likely to be in the neutral or negative charge state. This can be seen directly in Fig. 2d where a single electron switches between these two dangling bonds.

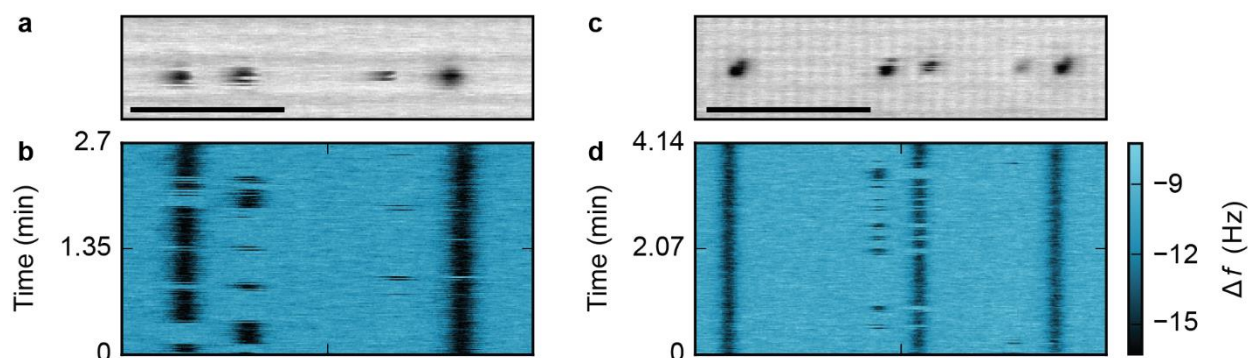


Figure S5: The influence of adding an isolated dangling bond on the polarization of dangling bond pairs. (a) Constant height Δf image of a symmetric structure composed of four dangling bonds. (b) A line scan map composed of two hundred sequential Δf line scans acquired over the structure demonstrate that it is naturally polarized. The negative charge confined to the left-hand pair favors the outer dangling bond but occasionally fluctuates to the inner dangling bond. The negative charge confined to the right-hand pair almost exclusively occupies the outer dangling bond. (c) An isolated dangling bond was added to the left of the *same* structure in (a) using STM lithography. (d) A line scan map composed of two hundred sequential Δf line scans acquired over the structure demonstrate the effect of this additional negative charge to the polarization of the structure. The right-hand pair remains polarized in the same way as (b). The polarization of the left-hand pair reverses compared to (b). This is easily rationalized by noting that the new dangling bond acts as a new local Coulombic bias. This demonstrates that local charges (e.g. negatively charged dangling bonds or ionized donors) can influence the distribution of charge states these structures display. The scale bars in (a) and (c) are 3 and 4 nm, respectively. The individual line scans acquired in (d) are longer than in (b) due to the increased distance the tip has to move. The Δf colour bar applies to both (b) and (d).

References

1. Giessibl, F. J. Atomic resolution on Si(111)-(7×7) by noncontact atomic force microscopy with a force sensor based on a quartz tuning fork. *Applied Physics Letters* **76** (11), 1470, doi:10.1063/1.126067 (2000).
2. Labidi, H. *et al.* New fabrication technique for highly sensitive qPlus sensor with well-defined spring constant. *Ultramicroscopy* **158**, 33–37, doi:10.1016/j.ultramic.2015.06.008 (2015).
3. Rezeq, M., Pitters, J. & Wolkow, R. Tungsten nanotip fabrication by spatially controlled field-assisted reaction with nitrogen. *The Journal of Chemical Physics* **124** (20), 204716, doi:10.1063/1.2198536 (2006).
4. Pitters, J. L., Piva, P. G. & Wolkow, R. A. Dopant depletion in the near surface region of thermally prepared silicon (100) in UHV. *Journal of Vacuum Science & Technology B, Nanotechnology and Microelectronics: Materials, Processing, Measurement, and Phenomena* **30** (2), 21806, doi:10.1116/1.3694010 (2012).
5. Haider, M. B., Pitters, J. L., DiLabio, G. A., Livadaru, L., Mutus, J. Y. & Wolkow, R. A. Controlled Coupling and Occupation of Silicon Atomic Quantum Dots at Room Temperature. *Physical Review Letters* **102** (4), 46805, doi:10.1103/PhysRevLett.102.046805 (2009).
6. Livadaru, L., Pitters, J., Taucer, M. & Wolkow, R. A. Theory of nonequilibrium single-electron dynamics in STM imaging of dangling bonds on a hydrogenated silicon surface. *Physical Review B* **84** (20), 205416, doi:10.1103/PhysRevB.84.205416 (2011).